Optical design and verification of the 4mm receiver for the 20m telescope at Onsala Space Observatory

Optical design and verification of a 4mm receiver for the 20m telescope at Onsala Space Observatory

George W. Walker, Eimante Kalinauskaite, Darragh N. McCarthy, Neil A. Trappe, Anthony Murphy, et al.

George W. Walker, Eimante Kalinauskaite, Darragh N. McCarthy, Neil A. Trappe, Anthony Murphy, Leif Helldner, Miroslav G. Pantaleev, Jonas Flygare, "Optical design and verification of a 4mm receiver for the 20m telescope at Onsala Space Observatory," Proc. SPIE 9914, Millimeter, Submillimeter, and Far-Infrared Detectors and Instrumentation for Astronomy VIII, 99142V (19 July 2016); doi: 10.1117/12.2232576

SPIE.

Event: SPIE Astronomical Telescopes + Instrumentation, 2016, Edinburgh, United Kingdom

Optical design and verification of a 4mm receiver for the 20m telescope at Onsala Space Observatory

George W. Walker[a], Eimante Kalinauskaite[a], Darragh N. McCarthy[a], Neil A. Trappe[a], Anthony Murphy[a], Leif Helldner[b], Miroslav G. Pantaleev[b], and Jonas Flygare[b]

[a]National University of Ireland, Maynooth, Co. Kildare, Ireland
[b]Onsala Space Observatory, Onsala, Sweden

ABSTRACT

The work of this research is the design, analysis and verification of the optical performance of a 4 mm receiver channel for the 20 m telescope at Onsala Space Observatory, Onsala, Sweden. The 4 mm (75 GHz) receiver is a newly proposed channel designed to be installed parallel to the existing 3 mm (100 GHz) channel targeting new science at that longer wavelength. Gaussian beam mode analysis is used to produce the fundamental optical design of the system. The design is then analysed more accurately with the physical optics approximation. We report on the comparison of simulation and measurement and verification of the system design.

Keywords: Optical design, Onsala Space Observatory, 4mm receiver, 20m telescope, Analysis, Verification, Gaussian, Physical Optics

1. INTRODUCTION

Onsala Space Observatory (OSO),[1] which was founded in 1949 by Olaf Rydbeck, is the Swedish National Facility for Radio Astronomy. It is associated with the Department of Earth and Space Scientists at Chalmers University of Technology. The 20 m telescope is enclosed in a 30 m diameter radome which protects it from the weather, and it follows a classical Cassegrain design.

The 4 mm receiver channel is being installed parallel to an existing 3 mm channel[2] in order to view frequencies in the 4 mm band. The 3 mm channel was designed to operate between 85 GHz and 116 GHz,[3] whereas the 4 mm receiver channel is to operate between 67 GHz and 86 GHz.

There primary requirements for the optical design are as follows: mechanical constraints associated with the design as the system is to fit within a cryostat unit; low cross polar levels; low power truncation at the optical components and windows; wavelength independent coupling between the horn aperture and the antenna subreflector rim, and edge taper of -12 dB at the secondary mirror.

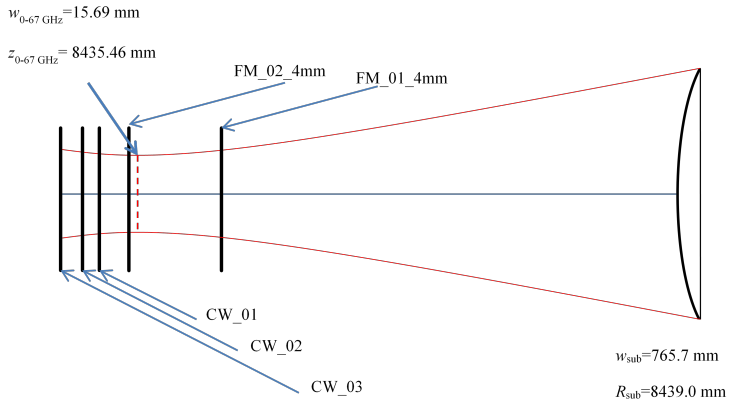

Figure 1: Simplified schematic showing position of mirrors and cryostat windows[2]

Millimeter, Submillimeter, and Far-Infrared Detectors and Instrumentation for Astronomy VIII, edited by Wayne S. Holland, Jonas Zmuidzinas, Proc. of SPIE Vol. 9914, 99142V

The 3 mm and 4 mm receiver channels are housed in a cryostat which is located near the telescope's focal point.[2] There is a sliding mirror mechanism for the on/off calibration of the 3 mm and 4 mm receiver channels. The flat reflectors in this part of the optical train have no effect on the beam, but incur an additional propagation distance which must be accounted for.

Figure 1 shows the position of the mirrors and cryostat windows, along with the propagation of a beam at 67 GHz. The first flat mirror after the antenna subreflector is referred to as FM_01_4mm and the second as FM_02_4mm. FM_02_4mm is located 146.394 mm from FM_01_4mm. It is tilted at an angle of 45°, and it directs the incident radiation into the cryostat. The beam must fit through a series of cryostat windows. The first of these is denoted CW_01. It has a diameter of 91 mm and is located a distance of 71.6 mm from FM_02_4mm. The second cryostat window, CW_02, has a diameter of 92 mm and is located a distance of 34.3 mm from CW_01. CW_03 is the third cryostat window, and has a diameter of 95 mm and is located at a distance of 43.2 mm from CW_01.

The geometrical constraints affecting the design within the cryostat unit are shown in figure 2. CM_01_4mm is an ellipsoidal mirror on an axis in line with the cryostat window, and CM_02_4mm is an ellipsoidal mirror on the axis in line with the horn. The horn aperture is imaged by CM_02_4mm to a focus between CM_02_4mm and CM_01_4mm, and this is then imaged to the secondary mirror. The final design for the conical corrugated horn has a slant length of 100 mm and an aperture radius of 15 mm.

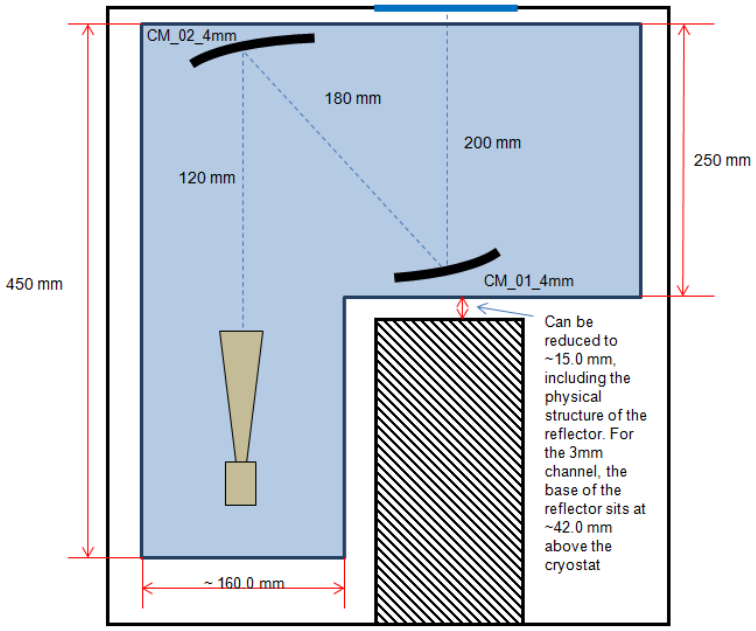

Figure 2: Geometrical constraints for the 4 mm system

2. FUNDAMENTAL OPTICAL DESIGN

Gaussian beam mode analysis (GBMA) plays an important role in the design and verification of quasioptical systems. In this project, it is used for the fundamental optical design of the system, as it is a computationally efficient method which provides all critical beam characterization through the optical train.

Gaussian beams are beams of electromagnetic radiation in which the transverse electric field and intensity are well approximated by Gaussian functions.

The paraxial wave equation is the basis for Gaussian beam propagation.[4] This makes the assumption that the variation of the amplitude along the direction of propagation will be small over distances comparable with the wavelength, and that the axial variation will be small compared with the perpendicular variation.

In a quasioptical system, such as the 4 mm receiver, there will be elements such as mirrors and lenses which alter the properties of the Gaussian beam. Ray transfer matrix analysis, which is adapted from geometrical analysis, is used to model this beam transformation. This is also known as ABCD matrix analysis due to the use of these letters to denote the matrix elements.

ABCD matrix analysis is extremely useful in quasioptical analysis, as it means that the ray theory of geometrical optics can be applied to the Gaussian beam representation of a system. Each element of a system has a unique ABCD matrix; these are multiplied together to determine the overall system matrix. For this section, the system is treated as a linear system, and thin lenses are used to represent the mirrors.

The combined matrix for the system is

$$M = \begin{pmatrix} 1 & d_3 \\ 0 & 1 \end{pmatrix} \begin{pmatrix} 1 & 0 \\ -\frac{1}{f_2} & 1 \end{pmatrix} \begin{pmatrix} 1 & d_2 \\ 0 & 1 \end{pmatrix} \begin{pmatrix} 1 & 0 \\ -\frac{1}{f_1} & 1 \end{pmatrix} \begin{pmatrix} 1 & d_1 \\ 0 & 1 \end{pmatrix} \tag{1}$$

This was then used to determine the evolution of the optical beam at important planes in the system.

In order to cover the width of the channel, analysis was performed for three frequencies: 67 GHz, 76.5 GHz, and 86 GHz. The focal lengths were chosen so that the beam radius at the secondary mirror would be equal at all three frequencies, i.e. the system would be wavelength independent. Focal lengths of $f_1 = 56.07$ mm and $f_2 = 79.355$ mm were chosen for the two mirrors.

The beam waist forms a distance Δ behind the aperture, defined by

$$\Delta = \sqrt{\frac{w^2}{1 + \left(\frac{\pi w^2}{\lambda R}\right)^2}} \tag{2}$$

The following tables give the values of Δ, beam waist distance and width from mirror 2, and the beam width at the secondary mirror for the three frequencies.

Table 1: Δ, beam waist location and radius for the large horn

Frequency (GHz)	Δ (mm)	waist distance from M2 (mm)	w at waist(mm)	w at secondary (mm)
67	29.9683	308.66476	15.6784	767.093
76.5	35.8102	312.96890	13.7499	765.635
86	41.3504	315.94015	12.2423	764.632

3. ANALYSIS OF DESIGN USING PHYSICAL OPTICS

While Gaussian beam mode analysis is a good representation of beam propagation in quasioptical systems, it does not provide sufficient accuracy when precise detail of the beam propagation is required. For this reason, the Physical Optics (PO) technique is used. The PO technique is an approximation of the full electromagnetic solutions of Maxwell's equations. GRASP is an example of an electromagnetic simulation package which makes use of this technique.

Reflector objects are defined in GRASP using a surface object and a rim object. The rim describes the edge of the scatterer.

Elliptical reflectors are used here, to image a beam waist at one point to another point, as an ellipse has two focal points. Parabolic reflectors are used when parallel beams need to be brought to a focus, for example when collecting radiation from the sky. Parabolic reflectors are useful where parallel beams are required to be brought to a focus.

An ellipsoid is generated by rotating an ellipse about one of its axes. The distances R_1 and R_2 from the focal points to the point of reflection on the surface are related as follows:

$$\frac{1}{f} = \frac{1}{R_1} + \frac{1}{R_2} \tag{3}$$

where f is the the focal length determined from the ABCD matrices, where the mirrors are treated as lenses. Because this is a geometric design, R_1 is determined by adding the radius of the horn to the distance from the horn to the first mirror.

A beam from the first focal point will travel a distance of R_1 before reflecting off the surface and travelling a distance of R_2 to the second focal point.

Using R_1, R_2, and θ, the parameters of the ellipse can be determined, and the defining polynomial is implemented in GRASP as a 2nd order quadric polynomial surface. The origin is one of the vertices of the ellipsoid. The surface must then be rotated so the mirror is in the correct position.

The following three methods were used to define input horn fields.[5] Two of them are generated by GRASP, and the third uses an externally defined field.

The first method defines a feed which radiates a Gaussian beam using the near-field parameters of the Gaussian beam. It provides a field with a Gaussian taper, and it satisfies Maxwell's equations. This is used as a simple model for the radiation from a corrugated horn. A corrugated horn has 98% of its power in an equivalent Gaussian, which is scaled to the right size to represent it.

The beam radius w and the phase front radius are related to the beam waist w_0 and the position of the waist at $-z_0$ by

$$w = w_0\sqrt{1 + z_0^2/b^2} \tag{4}$$

$$R_C = z_0(1 + b^2/z_0^2) \tag{5}$$

where the confocal distance $b = w_o^2 k/2$ and the wavenumber $k = 2\pi/\lambda$.

The Gaussian beams cuts at the secondary mirror are shown in figure 3. There is greater divergence from the Gaussian beam in the x cut because this is the plane in which the mirror reflection occurs. Here, the beams for the three frequencies are plotted on the same graph to show that the beam size is wavelength independent. There is good agreement with the expected Gaussian fit with a beam radius of 765.7 mm.

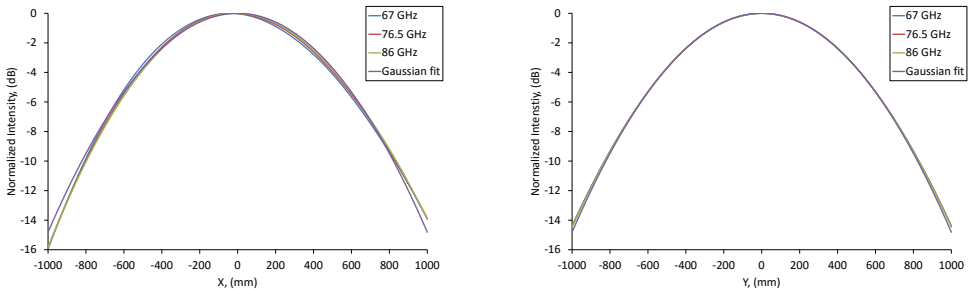

Figure 3: Cuts of the Gaussian beam at the Secondary Mirror, w=765.7 mm

From this, it can be concluded that the system images the horn aperture in a wavelength independent manner.

The hybrid mode conical horn is a more rigorous description of the radiation produced from a conical corrugated horn.[6] The horn is operating under the balanced-hybrid condition and has a narrow flare angle. The parameters required are the aperture radius, the semi-flare angle, and the distance to the phase centre of the horn. The hybrid modes HE_{mn} and EH_{mn}, and the cylindrical modes TE_{0n} and TM_{0n} are supported. The conical corrugated horn operates under the hybrid HE_{11} mode.

Figure 4 shows the cuts at the beam waist locations for when the GRASP Hybrid horn is used as a source. The cuts are graphed against a truncated Bessel field, which is a better match than the Gaussian field distribution.

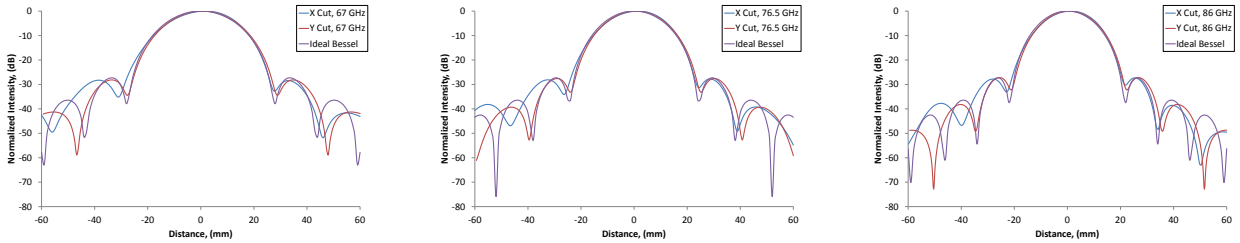

(a) 67 GHz (b) 76.5 GHz (c) 86 GHz

Figure 4: Cuts of the GRASP Hybrid Horn beam at the focal planes

Figure 5 shows the cuts taken at the position of the secondary mirror for the Hybrid mode horn. There is good agreement with the truncated bessel field, especially in the *y* cut.

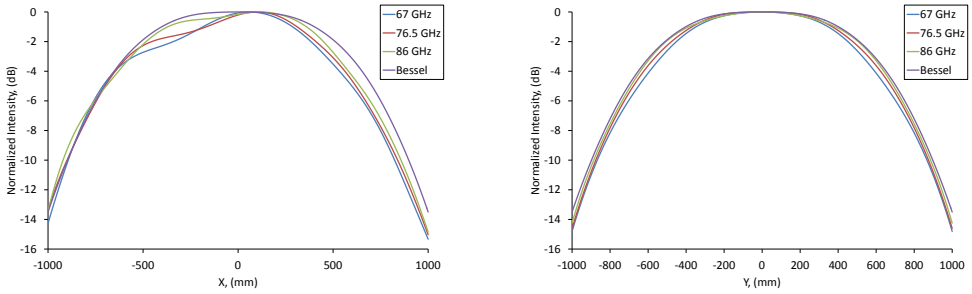

Figure 5: Cuts of the Hybrid Mode Horn at the Secondary Mirror

The third method of providing a source uses an external user defined input horn field. Grid files for the three frequencies were used. The grid files store field values in a rectangular grid. They were produced using the mode matching software *Scatter*, which was developed by the Terahertz Optics and Technology Group at Maynooth University.[7]

The basis of the mode matching technique used by *Scatter* is splitting a horn into segments of increasing radius, and considering the propagation of modes through each section. At each junction between sections of different radius, an overlap integral is performed to provide the level of coupling between the modes. The modes are then recombined to provide the resulting field.

Figure 6 gives the cuts taken at the beam waist location using the real aperture grid files as a tabulated planar source.

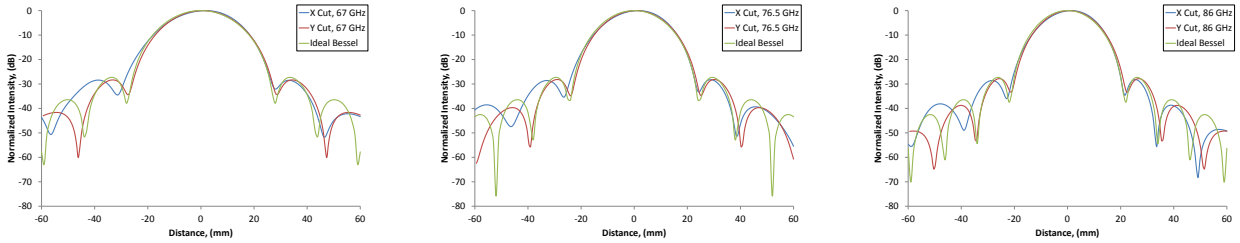

(a) 67 GHz (b) 76.5 GHz (c) 86 GHz

Figure 6: Cuts at the focal planes for the real horn grid files (with no transition)

The following contour plots in figure 7 were generated at the secondary mirror.

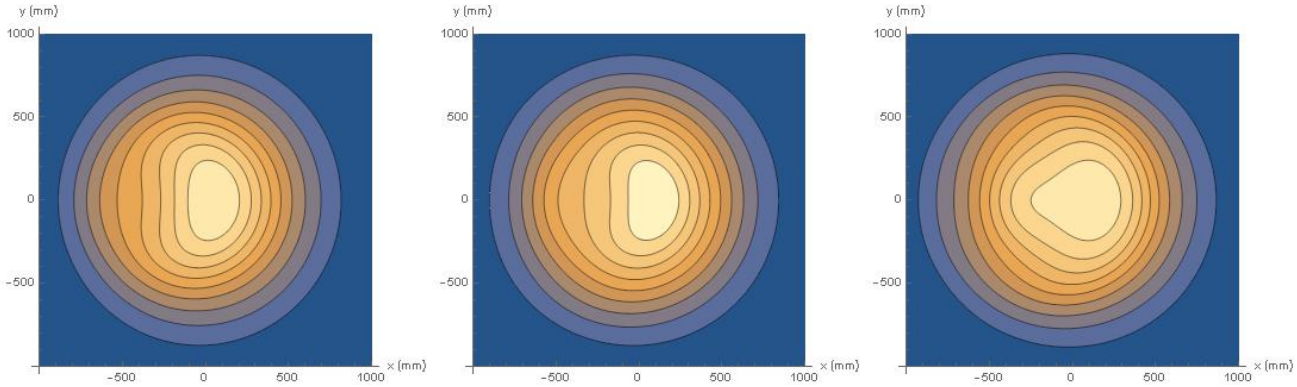

(a) 67 GHz (b) 76.5 GHz (c) 86 GHz

Figure 7: Contour plots at secondary

4. PROPAGATION OF BEAM TO THE SKY

While the beams plotted above at the secondary mirror have asymmetries, the primary interest to astronomers is the symmetry of the beam on the sky. Figure 8 shows an initial examination of the beam propagated to the sky at 67 GHz. This shows that the asymmetries are in the sidelobes, and that the main beam is now symmetric.

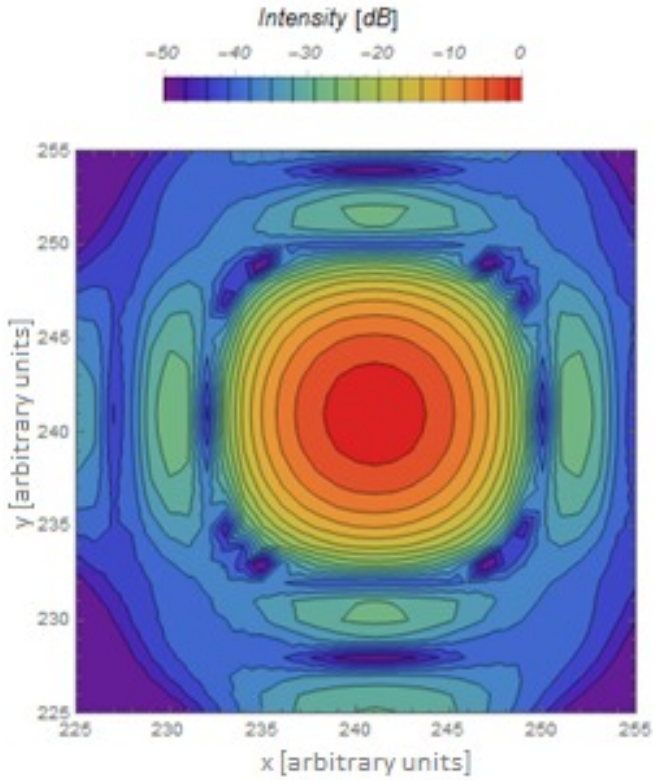

Figure 8: 67 GHz beam at the sky

5. OPTICAL EFFICIENCY AND CROSS-POLARIZATION

The optical efficiency is the coupling of the predicted beam from the detector horn with the beam from the sky at the subreflector. To achieve this, the predicted beam is coupled with a truncated plane field, also known as a top-hat field because of its shape. The top-hat field has a hole in the centre due to the design of the Cassegrain telescope, which blocks some of the incoming radiation due to the shadow of the secondary mirror on the primary mirror. The top-hat field has the same radius as the secondary mirror. The optical efficiency calculations are performed using the following equation.[8]

$$K_{00} = \left| \frac{\int_S F^* E_{00} ds}{\sqrt{\int_S F^* F ds \int_S E_{00}^* E_{00} ds}} \right| \tag{6}$$

Cross-polarization is polarization orthogonal to the intended co-polarization, i.e. the direction of the linearly polarized detectors. It is desirable to keep the cross-polar levels low. The cross-polar levels below were calculated by integrating the total power in the cross-polar beam and normalizing it relative to the co-polar beam. The beam was sampled at both the horn aperture and the secondary mirror. This is given by the following equation:

$$XsP = 10 \log_{10} \left[\frac{\varepsilon_{\text{xsp}}}{\varepsilon_{\text{cop}}} \right] \tag{7}$$

where XsP is the cross-polar level (in dB), and ε_{xsp} and ε_{cop} are respectively the power levels of the cross and co polar distributions. The modematching code accurately predicts co-polar and cross-polar levels of the horn, and GRASP allows full vector free space analysis.

Table 2: Beam efficiency and cross-polarization for the grid files

Frequency (GHz)	Beam Efficiency (%)	XsP at aperture (dB)	XsP at secondary (dB)
67	83.1208	-38.0564	-30.3578
76.5	83.7483	-41.5966	-31.992
86	84.2683	-38.9372	-32.6641

6. TRUNCATION ANALYSIS WITH THE ABCD CODE

The truncation analysis presented below is based on the ABCD code, but with the truncated beam based on the Bessel function accounting for losses at the edges of the beam due to the size of the mirrors and cryostat windows.

Table 3: Comparison of beam efficiency for both the untruncated and truncated beams

Frequency (GHz)	Untrunc. Efficiency (%)	Trunc. Efficiency (%)
67	0.852283	0.838773
76.5	0.852283	0.84434
86	0.852283	0.843619

Truncation of the beam causes a slight reduction in coupling efficiency, which is to be expected.

7. COMPARISON WITH THE 3MM SYSTEM

As the 4 mm system based on an upgrade to a previous system operating at wavelengths around 3 mm, it was important to compare the operation of the 4 mm system with that of the existing 3 mm design. The 3mm design was constructed using a 100 mm horn-cryostat separation and with a horn having a 12 mm aperture and a 97.73 mm slant length. It was designed to operate between 85 and 116 GHz.

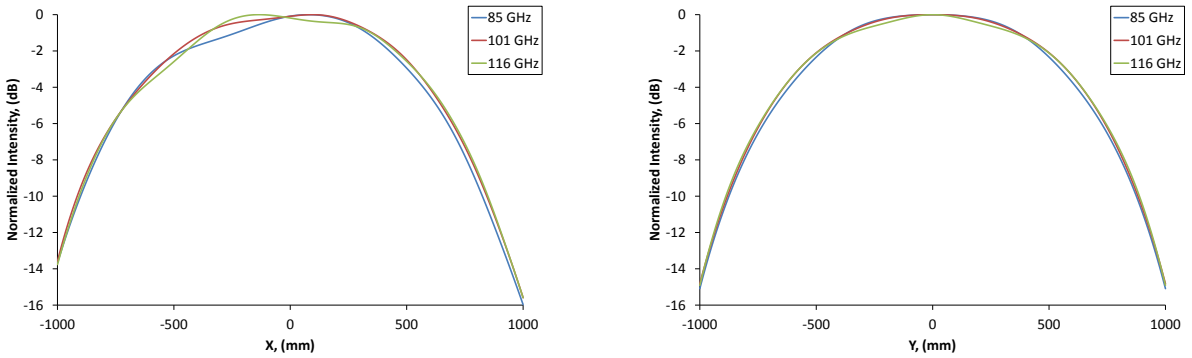

Figure 9: Cuts of the Hybrid Mode Horn at the Secondary Mirror for the 3mm system

Cuts of the Hybrid Mode horn at the Secondary Mirror are shown for the 3mm system in Figure 9. Similar aberrations to the new 4mm system can be seen in the x cut.

8. EXPERIMENTAL MEASUREMENTS

The system was manufactured in Autumn 2015, and initial test measurements were made.[9] A pyramidal test horn was used during the test measurements, so it was necessary to convolve the horn beam pattern with that of the GRASP simulation in order to compare like with like. Using the convolution theorem, the convolved beam is found from the Fourier transforms of the two component beams:[10]

$$[f * g] = \mathscr{F}^{-1}\left[\mathscr{F}[f].\mathscr{F}[g]\right] \tag{8}$$

where $*$ represents convolution and $\mathscr{F}$ is the Fourier transform.

The aperture field for the pyramidal horn is given by[11]

$$E_y = E_0 \cos\frac{\pi x}{A} \exp\left[-i\frac{k}{2}\left(\frac{x^2}{R_1^2} + \frac{y^2}{R_2^2}\right)\right] \tag{9}$$

where R_1 and R_2 for the test horn are 40.33 mm and 37.24 mm respectively.

There was also some misalignment between the origin of the test horn and that of the 4 mm receiver window. Measurements found the offset of the receiver with respect to the test horn to be $x = -5.5$ mm and $y = 2.25$ mm. There was also an angular misalignment which resulted in the test horn pointing approximately 0.382° in the positive x direction. The misalignment was accounted for in GRASP by modifying the coordinates of the output grid. A typical experimental result is shown in figure 10, along with the GRASP simulated beam, and the convolution of the GRASP beam and the aperture field of the test horn. The graph shows how the convolution modifies the position of the feature to be in the same position as the experimental result.

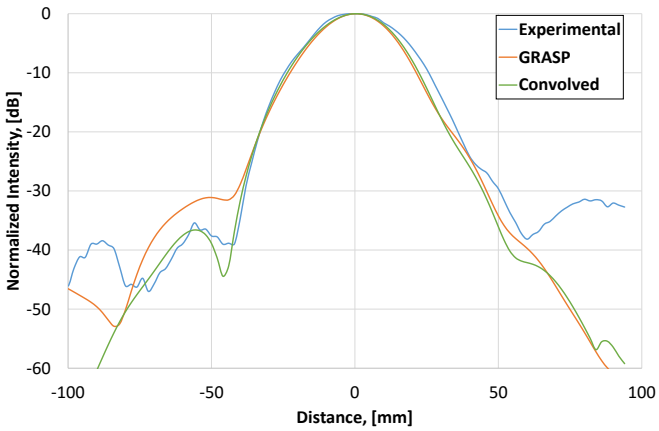

Figure 10: Example of experimental result compared with GRASP and convolved beam (69 GHz, x cut)

ACKNOWLEDGMENTS

The author wishes to acknowledge financial support from the European Space Agency through the Special Strategic AO for Ireland.

REFERENCES

[1] O. S. Observatory, "*About us.*" http://www.chalmers.se/en/centres/oso/about-us/Pages/default.aspx.

[2] M. Whale, "*OSO 4mm Receiver - Notes on Optical Design & Prescribed Work Packages.*" 2014.

[3] O. Nyström, *Design, Characterization, and Calibration of Low-Noise Terahertz Receivers.* PhD thesis, Chalmers University of Technology, 2011.

[4] P. F. Goldsmith, *Quasioptical Systems: Gaussian Beam Quasioptical Propagation and Applications*, IEEE Press, 1998.

[5] TICRA, *GRASP9 Reference Manual*, 2010.

[6] M. Whale, *Optical Characterisation of Astronomical Submillimetre Receivers including ALMA Bands 5 and 9.* PhD thesis, National University of Ireland, Maynooth, 2010.

[7] S. Doherty, *Optical and Quasi-Optical Design and Analysis of Astronomical Instrumentation including a Prototype Safari Pixel.* PhD thesis, National University of Ireland, Maynooth, 2012.

[8] M. Candotti, *Design, Analysis and Optimisation of Quasi-Optical Systems for Sub-mm Astronomy Instrumentation.* PhD thesis, National University of Ireland, Maynooth, 2007.

[9] J. Flygare, "*OSO 4mm Test Setup and Notes.*" 2015.

[10] E. W. Weisstein, "*Convolution Theorem.*" http://mathworld.wolfram.com/ConvolutionTheorem.html. From MathWorld–A Wolfram Web Resource.

[11] S. Drabowitch, A. Papiernik, H. Griffiths, and J. Encinas, *Modern Antennas*, Chapman & Hall, 1998.